

Wavelet graphs for the direct detection of gravitational waves

Eric CHASSANDE-MOTTIN¹, Eric LEBIGOT^{1,2}, Hugo MAGALDI¹, Eve CHASE¹, Archana PAI³, Gayathri V³, Gabriele VEDOVATO⁴

¹APC, Univ Paris Diderot, CNRS/IN2P3, CEA/Irfu, Obs. de Paris, Sorbonne Paris Cité, France

²Tsinghua University, Beijing, China

³IISERTVM, Computer Science Building, CET Campus, Trivandrum Kerala, India

⁴INFN, Sezione di Padova, Padova, Italia
ecm@apc.univ-paris7.fr

Résumé – Une seconde génération de détecteurs d’ondes gravitationnelles entrera prochainement en fonction avec l’objectif de mesurer pour la première fois le faible signal gravitationnel provenant de la coalescence de binaires de trous noirs et/ou d’étoiles à neutrons. Dans cette communication, nous proposons une méthode de recherche temps-fréquence alternative au filtre adapté habituellement utilisé pour détecter ce signal. Cette méthode repose sur l’utilisation d’un graphe qui encode, en créant des liens entre les coefficients de la décomposition temps-fréquence multi-échelle des données, l’évolution temporelle du signal ainsi que sa variabilité. Nous donnons une preuve de concept de l’approche proposée.

Abstract – A second generation of gravitational wave detectors will soon come online with the objective of measuring for the first time the tiny gravitational signal from the coalescence of black hole and/or neutron star binaries. In this communication, we propose a new time-frequency search method alternative to matched filtering techniques that are usually employed to detect this signal. This method relies on a graph that encodes the time evolution of the signal and its variability by establishing links between coefficients in the multi-scale time-frequency decomposition of the data. We provide a proof of concept for this approach.

1 Context and motivation

Einstein’s theory of General Relativity introduces the concept of a deformable and evolving space-time. The dynamics of space-time is prescribed by Einstein’s equations. In the linearised gravity framework (space-time metric is a small perturbation to the Minkowsian flat space-time metric), the Einstein’s equations can be transformed into the wave equation. The metric perturbation evolve and propagate like radiation with amplitude scaled as $1/r$ and travels with speed of light. These are referred to as *gravitational waves* (GW) as they propagate as disturbances of space-time itself [9]. GWs have never been directly detected so far, i.e., through the measurement of their effect on a man-made instrument.

The direct search for GWs has made significant progress with the advent of dedicated instruments based on high-precision laser interferometry. A worldwide network of kilometric-scale interferometric GW detectors including the US-based LIGO[1], the French-Italian project Virgo[2] completed a first series of science data collection over the past decade and will soon resume to take data in an advanced (ten times more sensitive) configuration. The first discovery of GWs is expected within the decade; this will open an entirely new view of the universe.

Those instruments are designed to sense the tiny space-time strain distortion inside the detector enclosure caused by GW

from distant astrophysical sources. Coalescing binaries of neutron star and/or black holes (in short, CBCs for compact binary coalescences) are one of the most promising sources of GW. The last minutes before the binary merges coincide with the emission of an intense burst of GWs. An accurate modeling of the dynamics of the binary shows that the GW waveform is a quasi-periodic signal, or chirp. The chirp frequency sweeps towards high values according to a power law. The baseline approach is to use this morphological information to search the data with matched filtering techniques (see e.g. [3]).

A large amount of computational resources is required to complete the search. This results from the combined effect of the large volume of data and physical signal parameter space to be searched and the impossibility to accurately model the instrumental noise. This implies that the analysis background has to be estimated empirically by repeating the analysis many (typ. 10^5) times on surrogate data obtained by shifting data streams with non-physical time delays.

In this article we propose a new wavelet-based method, alternative to matched filtering, to search for CBC signals. It relies on the multi-scale representation of CBC chirps using wavelet graphs (introduced in Sec. 2). The method is integrated in the data analysis pipeline Coherent WaveBurst that we present in the next section.

1.1 Multi-scale coherent transient searches

A whole range of data analysis pipelines has been developed for searching for GW transients (including CBC signals) through a combined analysis of multiple detector data. Among these, an important pipeline is Coherent WaveBurst (cWB) [7].

In a nutshell cWB extracts clusters of significant coefficients from time-frequency decompositions that results from the *coherent* combination of the data using sensor array techniques analog to beam-forming. The resulting clusters form candidate GW “events” if their “coherent” to “incoherent” signal energy ratio exceeds a threshold. We now detail how the time-frequency representations is computed and how the clusters are formed.

1.1.1 Multi-scale Wilson transform

In cWB’s scheme, the data (time series) are mapped into a set of time-frequency representations by projecting onto Wilson bases [5] which are a variation of the well-known Gabor bases. A Wilson basis is composed of linear phase cosine modulated wavelets distributed on a regular time-frequency lattice. According to [8] a pair of in-phase and quadrature orthonormal Wilson bases is constructed. Time-frequency maps are computed by summing the powers in the in-phase and quadrature transforms. A collection of maps is computed using the Meyer scaling function [8, 5] with different *scales* (i.e., wavelet duration or time scale). At scale a , the time-frequency lattice includes $a+1$ frequency subbands and N/a time bins where N is the number of data samples (typ., $N = 2^{20}$ i.e, 1024 s duration sampled at $f_s = 1024$ Hz).

The collection of time-frequency at all scales results in a three-dimensional redundant representation that spans the t, f and a variables. In the cWB scheme, the selected N_a scales are distributed dyadically, typ. $\log_2 a \in \{3, \dots, 8\}$. The total number of (t, f, a) pixels is $\sim N_a N \approx 6 \times 10^6$.

1.1.2 Transient extraction from Wilson transform

Significant pixels in the time-frequency-scale representation are selected by thresholding. In each time-frequency maps, the selected pixels are clustered using a nearest neighbour algorithm. The time-frequency clusters obtained at all scales are then combined using an algorithm that selects the principal components. This procedure does not make any prior assumption on the cluster geometry which can have an arbitrary shape in principle.

Because of their specific phase evolution, chirp signals have structured time-frequency representations with energy mostly concentrated on the instantaneous frequency curve (see e.g., [6]) thus leading to clusters of significant pixels with a specific shape. *We propose here a new clustering algorithm that targets that shape.*

2 Wavelet graphs

In this section, we determine the time-frequency-scale curve referred to as *chirp path* that collects the large wavelet coefficients associated to a given chirp signal. In presence of stationary noise, the coefficients in the path are the one which maximizes the signal-to-noise ratio locally.

We construct a graph that combines the paths from a family of chirp signals that covers a region of the parameter space. This wavelet graph is a central piece of the clustering algorithm we propose.

2.1 Chirp expansion in Wilson bases

For a given analysis frequency, we now determine which wavelet in the Wilson basis has the maximum coupling with the considered chirp.

Instead of using discrete Wilson transforms with Meyer wavelets as cWB, we work in the continuous time, frequency and scale limit and use sine Gaussian wavelets to allow analytical calculations. The wavelet at time t_0 , frequency f_0 and scale a_0 reads $\tilde{w}_0(f) = \tilde{g}(f - f_0; a_0) \exp -2\pi i f t_0$ where $\tilde{g}(\cdot)$ is the wavelet envelope assumed to be

$$\tilde{g}(f; \sigma_0) = (2\pi)^{1/4} \sqrt{\sigma_0} \exp -\pi^2 \sigma_0^2 (f - f_0)^2. \quad (1)$$

The scale parameters in the discrete/Meyer and continuous/Gaussian cases are approximately related by $a_0 \approx f_s \sigma_0$ where f_s is the sampling frequency.

The time-frequency map is defined as

$$\rho_0^2 \equiv \rho^2(t_0, f_0, a_0) = \left| \int df \frac{\tilde{w}_0^*(f) \tilde{s}(f)}{\tilde{N}(f)} \right|^2 \quad (2)$$

where $\tilde{N}(f)$ is the noise power spectrum. We seek the time t_0 and scale a_0 (or equivalently σ_0) which maximize ρ_0 for a given f_0 .

Chirps (including CBC signals) can be expressed as $\tilde{s}(f) = A(f) \exp i\Psi(f)$ in the Fourier domain. This allows us to rewrite Eq. (2) as an oscillatory integral. We then evaluate this integral with the stationary phase approximation [4] assuming slow variations of the integrand amplitude with respect to its phase. We obtain :

$$\rho_0^2 \approx \frac{\pi |A(f_0)|^2}{|\pi^2 \sigma_0^2 - i\beta|} \exp \left[\Re \frac{\pi^2 (t_0 - \tau(f_0))^2}{\pi^2 \sigma_0^2 - i\beta} \right], \quad (3)$$

where $\mathcal{A}(f) = (2\pi)^{1/4} \sqrt{\sigma_0} A(f) / \tilde{N}(f)$, $\beta = \ddot{\Psi}(f_0)/2$ and $\tau(f_0) = -(2\pi)^{-1} \dot{\Psi}(f_0)$ denotes the inverse chirp rate and group delay, resp.

The maximization of this quantity in t_0 and σ_0 at the given frequency yields

$$\rho^2(\hat{t}_0, f_0, \hat{a}_0) = \frac{f_s |A(f_0)|^2}{\sqrt{\pi} \hat{a}_0 \tilde{N}(f_0)}, \quad (4)$$

with the maximum reached at $\hat{t}_0 = \tau(f_0)$ and $\hat{\sigma}_0 = \sqrt{|\beta|}/\pi$ converted into \hat{a}_0 using the Gaussian to Meyer scale conversion stated above.

We conclude that the chirp path is the following curve in the time-frequency-scale space parametrized by the frequency f_0

$$\hat{t}_0 = -\frac{1}{2\pi}\dot{\Psi}(f_0) \quad \hat{a}_0 = \frac{f_s}{\sqrt{2\pi}}\sqrt{|\ddot{\Psi}(f_0)|}. \quad (5)$$

The last expression implies that signals with slowly (resp. rapidly) varying frequency are best approximated by wavelets of large (resp. small) scale as expected intuitively.

The chirp path essentially depends on the chirp Fourier phase $\Psi(\cdot)$. For CBC chirp signals, this phase in the *Newtonian* approximation is [9]

$$\Psi(f) = \psi_c - 2\pi f t_c - \frac{6\pi f_L \tau_0}{5} \left(\frac{f_L}{f}\right)^{5/3}, \quad (6)$$

where ψ_c is the final phase at coalescence time t_c . The chirp duration τ_0 from the lower cut-off f_L to maximum frequency reads

$$\tau_0 = \frac{5}{256} \left(\frac{c^3}{GM}\right)^{5/3} (\pi f_L)^{-8/3}. \quad (7)$$

where the *chirp mass* $\mathcal{M} = (m_1 m_2)^{3/5} / (m_1 + m_2)^{1/5}$ depends on the binary component masses m_1 and m_2 .

Eqs. (5) thus leads to

$$\hat{t}_0 = t_c - \tau_0 \left(\frac{f_0}{f_L}\right)^{-8/3} \quad \hat{a}_0 = \frac{4f_s}{\sqrt{6}\pi} \left(\frac{\tau_0}{f_0}\right)^{1/2} \left(\frac{f_0}{f_L}\right)^{-4/3}.$$

We verify that the signal enters the detector frequency band ($f_0 = f_L$) at the arrival time $\hat{t}_0 = t_c - \tau_0$ and leaves it close to coalescence time.

Eqs. (5) provide approximations in the continuous limit. This curve has to be discretized according to the (t, f, a) lattice adopted by cWB. Discrete time and frequency coordinates read $\tilde{t}_0 = \lfloor \hat{t}_0 / \delta \rfloor \delta$ and $\tilde{f}_0 = \lfloor \hat{f}_0 \delta \rfloor / \delta$ and are obtained using the time sampling step $\delta = \bar{a}_0 / f_s$ at the discrete scale $\log_2 \bar{a}_0 = \lfloor \log_2 \hat{a}_0 \rfloor$ where $\lfloor \cdot \rfloor$ is the round-off operator. This results in a finite and ordered pixel collection with coordinates $(\tilde{t}_0, \tilde{f}_0, \bar{a}_0)$ we refer to as *chirp path*.

2.2 Cover chirp space with a graph

In the above model of Eq. (6), the coalescence time t_c and component masses m_1 and m_2 are not known *a priori* and have to be estimated from the data. For that reason, the chirp paths associated to the time and mass parameter space are computed and combined into the *wavelet graph* that collects the selected pixels and their connection with the previous pixel in the path (if any), referred to as *ancestor*. The last pixel of all paths is marked as an *end node*. If a pixel occurs in two (or more) chirp paths, the graph retains the list of all its ancestors.

Fig. 1 shows a typical wavelet graph computed for the mass range $m_1, m_2 \in [2.5, 10]M_\odot$ (expressed in unit of solar mass) and $t_c - t_{\text{ref}} \in [0, \delta_{\text{max}}]$ with $\delta_{\text{max}} = a_{\text{max}} / f_s \approx 250$ ms with the standard cWB settings (see Sec. 1.1.1). We fix the analysis frequency bandwidth from 40 Hz to the Nyquist frequency.

Despite the reasonably large physical space covered (1275 different CBC signals were used in this computation), the wavelet graph has a moderate size (~ 1000 nodes) and complexity ($\lesssim 10$ ancestors per node).

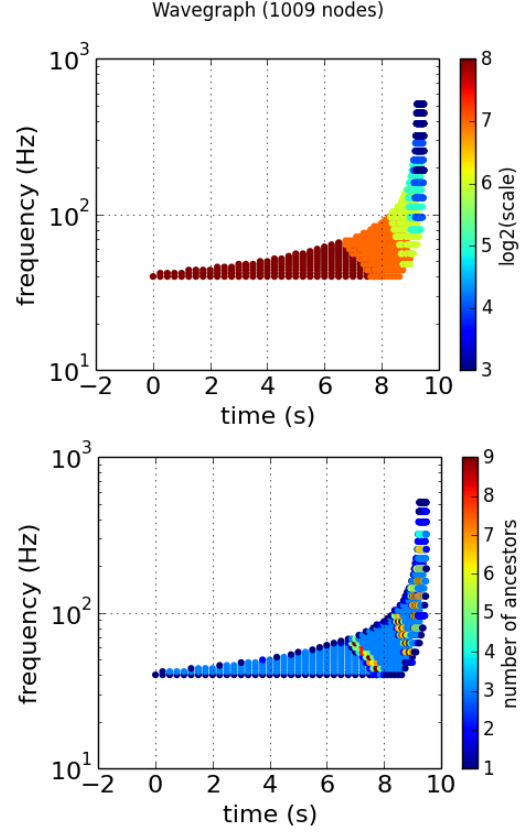


FIGURE 1 – Typical wavelet graph computed for CBC signal from binaries in the mass range $m_1, m_2 \in [2.5, 10]M_\odot$ (expressed in unit of solar mass). The top panel shows the distribution of selected pixel nodes in the (t, f, a) space. The bottom panel shows the number of ancestors per node.

3 Clustering with wavelet graphs

We now explain how the graph introduced in the previous section can be used to detect chirps in the data.

Assuming Gaussian noise, the detection of a known chirp signal can be performed optimally using matched filtering. The matched filtering statistics can be re-expressed in the wavelet domain. Assuming that the large coefficients of the chirp wavelet transform are essentially contained in the chirp path p obtained in Sec. 2.1 and that the selected wavelets in the chirp path are nearly orthogonal, this results in :

$$\ell(p) = \sum_{t,f,a \in p} \rho^2(t, f, a), \quad (8)$$

where the summation runs from the path start node (no ancestor) to the end node.

When the chirp parameters are unknown, this statistics has to be maximized over the admissible parameter space \mathcal{P} , namely $\max_{p \in \mathcal{P}} \ell(p)$. This maximization amounts to finding the chirp path in the wavelet graph that captures the largest amount of energy. That can be efficiently performed using combinatorial

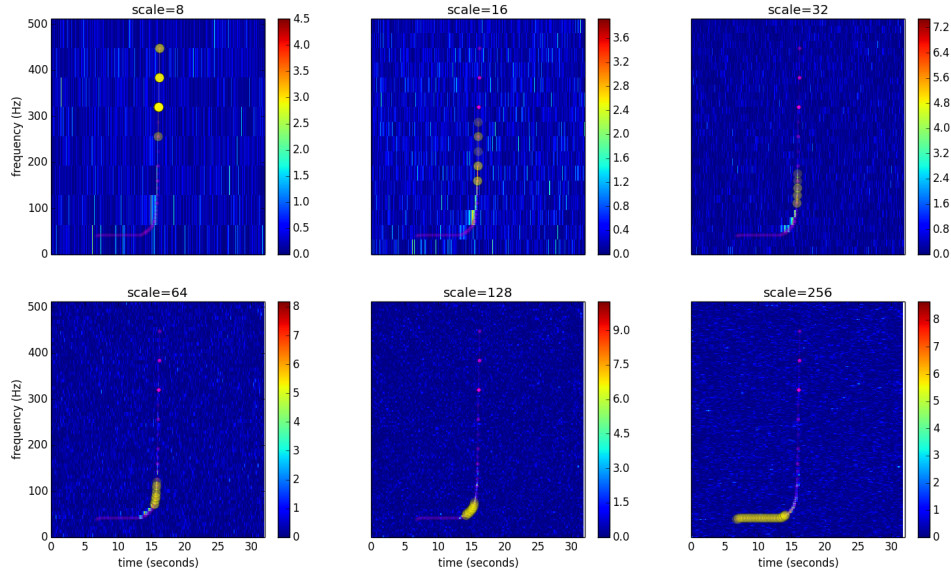


FIGURE 2 – Application of the proposed clustering method to a noisy CBC signal with $m_1 = m_2 = 5M_\odot$ using the wavelet graph in Fig. 1. The extracted cluster is shown in magenta with pixels at corresponding scale evidenced with yellow dots.

optimization techniques such as dynamic programming with a computing cost scaling linearly with the size of the graph.

We divide the data stream into successive segments and compute their Wilson transform. We assign to the graph node the values of the corresponding coefficients in the Wilson transform, apply dynamic programming to extract the “best” chirp path and move to the next segment. Chirp paths with ℓ exceeding a pre-defined threshold are retained and given to cWB as interesting clusters for further processing.

4 Concluding remarks

As an illustration, Fig. 2 presents the result of the wavelet graph clustering method on a CBC chirp signal in Gaussian white noise at large SNR ~ 60 . The cluster being continuous across times, frequencies and scales by design, it collects marginally significative pixels (because of noise fluctuations) which are lost otherwise in the standard cWB scheme.

Thanks to moderate graph size, the overall computing cost is in the acceptable range for production. On-going simulations will allow a full evaluation, beyond the present proof of concept.

Acknowledgements

We thank Sergey Klimenko for the access to the coherent WaveBurst software and Francesco Salemi for his useful comments on this work. We acknowledge the National Science Foundation (Award 1005036 through the University of Florida International REU for Gravitational Waves) and CNRS (PICS) for their support.

References

- [1] J Aasi et al. Advanced LIGO. *Class. Quantum Grav.*, 32(7) :074001, 2015.
- [2] F Acernese et al. Advanced Virgo : a second-generation interferometric gravitational wave detector. *Class. Quantum Grav.*, 32(2) :024001, 2015.
- [3] E. Chassande-Mottin. Data analysis challenges in transient gravitational wave astronomy. In *AIP Conf. Proc. : Acoustic and Radio EeV Neutrino Detection Activities, ARENA'12*, volume 1535, page 252, Erlangen (Germany), 2012.
- [4] T Dal Canton et al. Effect of sine-Gaussian glitches on searches for binary coalescence. *Class. Quantum Grav.*, 31 :015016, 2014.
- [5] I. Daubechies. *Ten Lectures on Wavelets*. Number 61. SIAM, 1992.
- [6] N. Delprat et al. Asymptotic wavelet and Gabor analysis : extraction of instantaneous frequencies. *IEEE Trans. Info. Theory*, IT-38(2) :644–673, 1992.
- [7] S. Klimenko et al. Constraint likelihood analysis for a network of gravitational wave detectors. *Phys. Rev. D*, 72 :122002, 2005.
- [8] V. Nacula et al. Transient analysis with fast Wilson-Daubechies time-frequency transform. *J. Phys. Conf. Ser.*, 363 :012032, 2012.
- [9] K.S. Thorne. Gravitational radiation. In S. W. Hawking and W. Israel, editors, *300 Years of Gravitation*. Cambridge University Press, 1987.